THE JOURNAL OF PHYSICAL CHEMISTRY C

Article

pubs.acs.org/JPCC

Investigating the Surface Structure of γ-Al_2O_3 Supported WO_X Catalysts by High Field ^{27}Al MAS NMR and Electronic Structure Calculations

Chuan Wan,[†,‡] Mary Y. Hu,[†] Nicholas R. Jaegers,[†,§] Dachuan Shi,[†] Huamin Wang,[†] Feng Gao,[†] Zhaohai Qin,[‡] Yong Wang,[§] and Jian Zhi Hu*[,†]

[†]Pacific Northwest National Laboratory, Richland, Washington 99354, United States

[‡]College of Science, China Agricultural University, Beijing 100193, China

[§]Voiland School of Chemical Engineering and Bioengineering, Washington State University, Pullman, Washington 99163, United States

Supporting Information

ABSTRACT: The metal−support interaction in γ-Al_2O_3 supported WO_X catalysts is investigated by a combination of high field quantitative single pulse (SP) ^{27}Al MAS NMR spectroscopy, 2D MQMAS, $^{1}H-^{27}Al$ CP/MAS, and electronic structure calculations. NMR allows the observation of at least seven different Al sites, including a pentahedral Al site (Al_P), three different tetrahedral Al sites (Al_T), and three octahedral Al sites (Al_O). It is found that the Al_P site density decreases monotonically with an increased WO_X loading, the Al_O site density increases concurrently, and the density of Al_T sites remains constant. This suggests that the Al_P sites are the preferred surface anchoring positions for the WO_X species. Importantly, the Al_P site isotropic chemical shift observed for the unsupported γ-Al_2O_3 at about 38 ppm migrates to the octahedral region with a new isotropic chemical shift value appearing near 7 ppm when the Al_P site is anchored by WO_X species. Density functional theory (DFT) computational modeling of the NMR parameters on proposed WO_X/γ-Al_2O_3 cluster models is carried out to accurately interpret the dramatic chemical shift changes from which the detailed anchoring mechanisms are obtained. It is found that tungsten dimers and monomers are the preferred supported surface species on γ-Al_2O_3, wherein one monomeric and several dimeric structures are identified as the most likely surface anchoring structures.

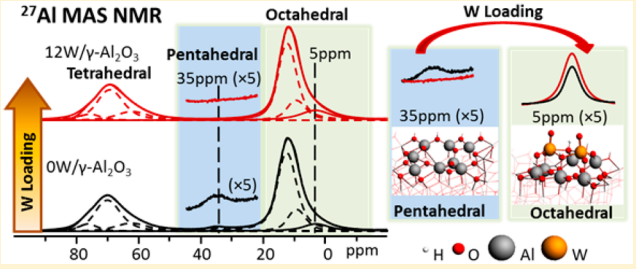

1. INTRODUCTION

The use of γ-alumina (γ-Al_2O_3) as an industrial catalyst and support in a wide variety of industrial processes[1−4] motivates scientific investigations into the nature of the interaction between the metal and the support surface, which has a profound influence on the catalytic activity.[5−7] As a model system, the interaction between a metal and the γ-Al_2O_3 surface has been a subject of fundamental studies for many years;[8,9] however, the highly disordered structure and the metastable nature associated with the commonly used industrial-grade, high surface area γ-Al_2O_3 make it quite challenging to investigate. Various experimental techniques, such as infrared (IR) spectroscopy, nuclear magnetic resonance (NMR) spectroscopy, X-ray diffraction (XRD), and transmission electron microscopy (TEM), have been used for structural characterization of γ-Al_2O_3.[10−14] The coordinatively unsaturated "defect sites", i.e., the penta-Al sites (Al_P), are believed to be the metal oxide anchoring positions;[14] however, there is still some debate regarding the structure of γ-Al_2O_3 supported metal/metal oxide catalysts. In particular, the nature of the surface interaction between a metal atom/metal oxide and the support surface in terms of the detailed atomic coordination is not fully established due to the lack of experimental evidence.[2]

NMR, a nondestructive and atom-specific tool, is ideal for such an investigation since the chemical shifts are highly sensitive to local structural changes. NMR can be used to study the detailed structural changes in both crystal and amorphous states and, notably, detect the presence of surface species. In fact, solid-state magic angle spinning (MAS) ^{27}Al NMR has been used extensively to investigate the structure changes associated with γ-Al_2O_3 supported metal catalysts such as Ba, Ni, Pt, Cu, etc., where single pulse (SP) experiments were carried out.[14−19] However, SP ^{27}Al NMR investigations are challenged by the lack of surface sensitivity. Both bulk structures (majority) and the surface species (minority) are observed simultaneously, and often the surface species are buried at the baseline or tails of the major peaks of the bulk structures making quantitative analysis challenging. This is particularly a problem when SP ^{27}Al MAS NMR experiments

Received: September 7, 2016
Revised: September 21, 2016
Published: September 26, 2016

DOI: 10.1021/acs.jpcc.6b09060
J. Phys. Chem. C 2016, 120, 23093−23103

are conducted at low magnetic field where line broadening from the second-order quadrupolar interaction becomes serious.[20,21] ^{27}Al MAS NMR experiments have been reportedly carried out at high fields of 19.975 and 21.1 T where remarkable spectral resolution can be obtained, allowing Al^{3+} cations in octahedral (Al_O), pentahedral,[22] and tetrahedral (Al_T) coordination to be clearly resolved. Even the fine structures among different Al_O sites can be observed.[14,23] With the help of the high field, Al_P has been identified as the anchoring sites for Al_2O_3 supported Pt catalyst,[14] where for the first time the decrease of the integrated Al_P peak intensity in a ^{27}Al MAS NMR spectrum was found to be correlated with the increase of the integrated peak intensity of the Al_O peak. Despite this interesting finding, the nature of the new Al_O sites remains unclear. Complimentarily, one can use multiple quantum (MQ) MAS ^{27}Al NMR to further increase the spectral resolution. The isotropic dimension of the two-dimensional MQMAS NMR spectrum is unperturbed by quadrupolar broadening, offering high spectral resolution along the evolution dimension. High resolution and clear assignation of the spectral features of Al_T, Al_P, and Al_O sites have been obtained with this technique even at low magnetic field.[23,24] To emphasize the contributions from surface species, the ^{1}H−^{27}Al cross-polarization (CP) MAS NMR experiments that are highly surface sensitive can be employed to probe Al sites that are near the surface OH groups.[23,25]

In this work, the γ-Al_2O_3 supported tungsten oxide (WO_X/γ-Al_2O_3) catalysts, which have been extensively used for olefin metathesis as a bifunctional catalyst,[8,26,27] were used to investigate the details of the metal−support interaction. Two types of γ-Al_2O_3, including a platelike Al_2O_3 with surface area of 56.9 m^2/g and a regular Al_2O_3 with surface area of 217.6 m^2/g both with varying amount tungsten oxide (WO_X) loadings, were analyzed. Single pulse ^{27}Al MAS NMR and MQMAS ^{27}Al NMR were conducted to analyze the bulk alumina, and the ^{1}H−^{27}Al CP MAS NMR was carried out to obtain information on the local environment of surface Al species. Furthermore, electronic structural calculations of the ^{27}Al chemical shifts using density functional theory (DFT)[28−34] were used to accurately assign the NMR signals and related the experimental results to the detailed interaction between tungsten and alumina surface environment. The combined analyses reveal unambiguously how the tungsten oxide interacts with the surface Al sites of γ-Al_2O_3.

2. EXPERIMENTAL SECTION

2.1. Sample Preparations. The platelike γ-Al_2O_3 was prepared by calcining a boehmite precursor (Catapal-200 from Sasol) at 800 °C in ambient air using a box furnace. Regular γ-Al_2O_3 was obtained from Sasol (Catalox SBa-200). The Brunauer−Emmett−Teller (BET) surface areas of these two materials are 56.9 m^2/g (platelike, named Series 1) and 217.6 m^2/g (regular, termed Series 2). The method of incipient wetness impregnation was used to obtain WO_X surface coverage ranging from 0.2 to 12 W atom/nm^2 (labeled as 0.2W/γ-Al_2O_3 to 12W/γ-Al_2O_3) and by using an aqueous solution of ammonium metatungstate hydrate (99.99%, Sigma-Aldrich) as a precursor. The sample without W (labeled as γ-Al_2O_3) was processed using the same method with pure water. The impregnated samples were dried in ambient air overnight and then were calcined at 450 °C in flowing dry air for 4 h. The sample information is summarized in Supporting Information Table S1.

2.2. NMR Measurements. All ^{27}Al MAS NMR experiments were performed at room temperature (20 °C) on a Varian-Inova 850 MHz NMR spectrometer with a commercial 3.2 mm HFXY probe, operating at a magnetic field of 19.975 T. The corresponding ^{27}Al Larmor frequency was 221.413 MHz. The 1D spectra were acquired at a sample spinning rate of 22 kHz using a commercial 3.2 mm pencil-type MAS probe. A single pulse sequence with a pulse width of 0.4 μs (corresponding to a solid $\pi/4$ pulse) and ^{27}Al radio-frequency (rf) field strength of 104.2 kHz (i.e., 2.4 μs for liquid $\pi/2$ calibrated by using 1 M $Al(NO_3)_3$ aqueous solution) was used. Each spectrum was acquired using a total of 2500 scans with a recycle delay time of 5 s and an acquisition time of 20 ms. The ^{27}Al 3Q MAS NMR (i.e., the MQMAS) spectra were obtained using a z-filter 3Q MAS pulse sequence,[35,36] i.e., the mqmas3qzf2d on a Varian-Agilent system, at a sample spinning rate of 20 kHz using the commercial 3.2 mm pencil-type MAS probe. The optimized pulse widths were pw1X = 2.4 μs and pw2X = 0.9 μs both at 104.2 kHz rf field strength and the selective pulse of pwXzfsel = 10.0 μs at rf field strength of 5.7 kHz. The pulse lengths for the three pulses were carefully optimized so that optimum MQMAS signal was obtained. In the hypercomplex 3Q MAS experiment, 96 transients for the real and imaginary F_1 FID were collected for each of the 90−192 evolution increments. The recycle delay was 2 s, and acquisition time was 10 ms. Spectral widths for the F_2 (acquisition) and F_1 (evolution) dimension were 250 and 40 kHz, respectively. The ^{1}H−^{27}Al CP NMR experiments were carried out at a rotor spinning rate of 20 kHz using the commercial 3.2 mm pencil-type MAS probe and ^{1}H rf field strength of 47.6 kHz for the $\pi/2$ pulse. The method of ramped CP was used for cross-polarization.[37] The CP match condition, including determining the optimal length of contact time, that generates the highest CP signal at 20 kHz spinning rate was carefully set up using the sample of boehmite (γ-AlO(OH)). Note that by using this standard a CP signal with good signal-to-noise ratio (about 10) was obtained using only one scan on 850 MHz if the CP match condition is accurately set. The optimized pulse width and contact time were 5.25 μs and 2 ms, respectively. Each CP spectrum was acquired using a total of 30K scans with a recycle delay time of 2 s and an acquisition time of 9.6 ms. All spectra were externally referenced to a 1 M $Al(NO_3)_3$ aqueous solution (0 ppm). The simulations of the spectra were performed using the Quadrupolar MAS 1/2 (Q mas 1/2) model implemented in the DMFIT program.[38]

2.3. Computational Method. The Amsterdam Density Functional (ADF-2014) package was used for electronic structure modeling. The geometry optimization was carried out using the generalized gradient approximation (GGA) based Becke−Lee−Yang−Parr function with dispersion functions (BLYP-D).[39] Furthermore, all the calculations were performed using the TZ2P basis set (triple ζ, two polarization functions) with the Slater-type functionals.[40] The large frozen core approximation, which demonstrated a similar accuracy to an all-electron solution,[40−43] was used to reduce the size of the basis set and therefore promote computational efficiency. For the calculation of NMR parameters, including chemical shift and quadrupolar coupling constant (C_Q), geometrically optimized structures at the same level of the theory and with the same basis set were employed.

DOI: 10.1021/acs.jpcc.6b09060
J. Phys. Chem. C 2016, 120, 23093−23103

The calculation of ^{27}Al NMR chemical shifts utilized α-Al_2O_3 as a secondary reference. Several clusters containing gradually increased numbers of Al atoms (10−56 Al atoms) were extracted from the crystal structure of α-Al_2O_3 from the American Mineralogist Crystal Structure Database,[44] and the geometries of the structures were fully optimized with terminal oxygen atoms charge balanced by adding hydrogen atoms. The NMR calculations were carried out on the geometry-optimized structures at the same level of the theory and with the same basis set. The calculated chemical shift values of the center Al atoms of α-Al_2O_3 were used to mimic the bulk α-Al_2O_3 coordination. The predicted absolute isotropic chemical shifts of the Al atoms in α-Al_2O_3 converged at 580 ppm. Since the experimental isotropic chemical shift value of bulk α-Al_2O_3 is located at 16 ppm with reference to 1 M $Al(NO_3)_3$ aqueous solution (0 ppm),[23] all the calculated shielding for Al atoms are converted using the equation

$$\delta_{iso} = \delta(\alpha\text{-}Al_2O_3) - \delta_{calc} + 16 = 580 - \delta_{calc} + 16 = 596 - \delta_{calc} \quad (1)$$

This chemical shift reference is further validated by direct calculations on $Al^{3+}(H_2O)_6$ clusters. The Al^{3+} ion coordinated with six H_2O molecules was used to mimic the Al^{3+} ion in dilute $Al(NO_3)_3$ aqueous solution. With the addition of H_2O molecules in a second solvation shell, the absolute chemical shielding of Al^{3+} in a $Al^{3+}(H_2O)_6(H_2O)_4$ structure is obtained as 598 ppm, where the second solvation shell of a Al^{3+} ion has four H_2O molecules. The value of 598 ppm is only 2 ppm higher than the 596 ppm given in eq 1, validating the use of eq 1. It should be noted that the use of eq 1 as the chemical shift reference is based on a prior literature report.[25] Detailed information regarding the calculations of α-Al_2O_3 and $Al^{3+}(H_2O)_6$ clusters is provided in the Supporting Information Figure S1.

3. RESULTS AND DISCUSSION

3.1. SP ^{27}Al MAS NMR on WO_X/γ-Al_2O_3 with Various W-Loadings. Figure 1 shows the center band SP ^{27}Al MAS NMR spectra for both the platelike and regular series of supported WO_X/γ-Al_2O_3 catalysts with different loadings of WO_X, i.e., 0−12 W atom/nm^2. Figure 1a was obtained with series 1 samples, and Figure 1b was obtained with series 2 samples. Both series have three peak regions at around 12, 35, and 70 ppm, which can be assigned to Al_O, Al_P, and Al_T site, respectively. Neither the peak positions nor the line shapes of Al_O or Al_T sites change significantly as a function of WO_X loading. However, the intensities of Al_P peaks decrease with increasing loading of WO_X for both series, indicating changes in the distribution and coordination of various surface WO_X species on the Al_P sites of these catalysts. This result strongly indicates that the Al_P sites are the primary sites responsible for the interaction between the WO_X and γ-Al_2O_3 surface.

3.2. MQMAS ^{27}Al NMR Spectra. The 2D MQMAS ^{27}Al NMR spectral study enables Al sites to be detected with greater detail. The results obtained on the 0W/γ-Al_2O_3 and 12W/γ-Al_2O_3 samples from both series are shown in Figure 2. Notably, the off-diagonal peaks in Figure 2 are due to the selection of a spectral width (i.e., 40 kHz) for the F_1 (isotropic) dimension that is twice the spinning rate of 20 kHz in order to observe the full isotropic spectral peaks along the F_1 (isotropic) dimension at high field of 850 MHz. By doing so, the first-order side bands associated with the octahedral and the tetrahedral aluminum sites were observed, accidentally appearing at around the

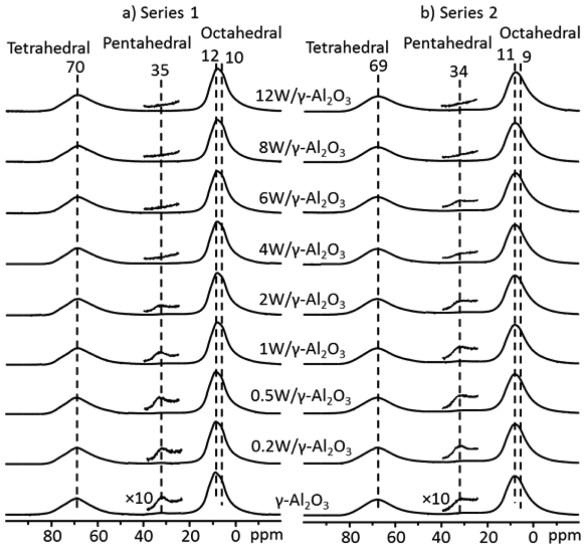

Figure 1. Center band spectra of SP ^{27}Al MAS NMR spectra of the γ-Al_2O_3 samples with various WO_X loadings of (a) platelike series 1 and (b) regular series 2. All of the 1D spectra were acquired with 2500 scan at 22 kHz spinning rate. Label scheme: γ-Al_2O_3 indicates γ-Al_2O_3 samples with 0 W atom/nm^2 loading, and 12W/γ-Al_2O_3 indicates γ-Al_2O_3 samples with 12 W atom/nm^2 loading, etc.

positions of diagonal peaks. The high quality of a 2D MQMAS has previously been demonstrated on H-Beta dehydration/rehydration experiments.[45] Seven Al sites with substantially different line shapes can be unambiguously detected. Three peaks can be identified in the Al_T region (85 to 60 ppm) with their peak centers located at about 65, 70, and 78 ppm. Likewise, three peaks can also be found in the Al_O regions (25 to 0 ppm) with their peak centers located at about 5, 10, and 12 ppm. A shoulder peak at about 0 ppm is clearly observed with significantly increased peak intensity for the higher WO_X loaded samples. In addition, the Al_P sites are observed in the parent samples (0 W atom/nm^2 loading) of the two series, and the center of the Al_P peak is around 35 ppm, consistent with 1D NMR (see Figure 1).

To gain further insight into the quantitative spectral information on the γ-Al_2O_3 supported WO_X with different W-loadings, sliced spectra can be cut parallel to the F_2 (anisotropic) dimension at various F_1 (isotropic) chemical shifts to observe the detailed changes of the peaks. Each sliced spectrum can be fit using one or two simple quadrupolar line shapes from which the isotropic chemical shift value, quadrupolar coupling constant (C_Q), and associated asymmetry factor (η_Q) can be determined. By progressively incrementing the F_1 values, simulations of the sliced spectra can distinguish three classes of quadrupolar line shapes in the Al_O spectral region, three in the Al_T region, and one in the Al_P region for both two series. The detailed fittings of the sliced spectra are shown in Figure S2, and the simulated result parameters are summarized in Table S2. As shown in Figure 2, four slices from F_1 chemical shift at about 0 ppm were selected to demonstrate the significant line shape change. Obviously, the most upfield peaks (isotropic chemical shift at about 7 ppm) of the 12 W atom/nm^2 loading samples in both series are significantly enhanced compared with their corresponding parent γ-Al_2O_3 samples.

3.3. SP ^{27}Al NMR Spectra Fitting. Using the known C_Q, η_Q, and isotropic chemical shift values from 2D MQMAS ^{27}Al

DOI: 10.1021/acs.jpcc.6b09060
J. Phys. Chem. C 2016, 120, 23093−23103

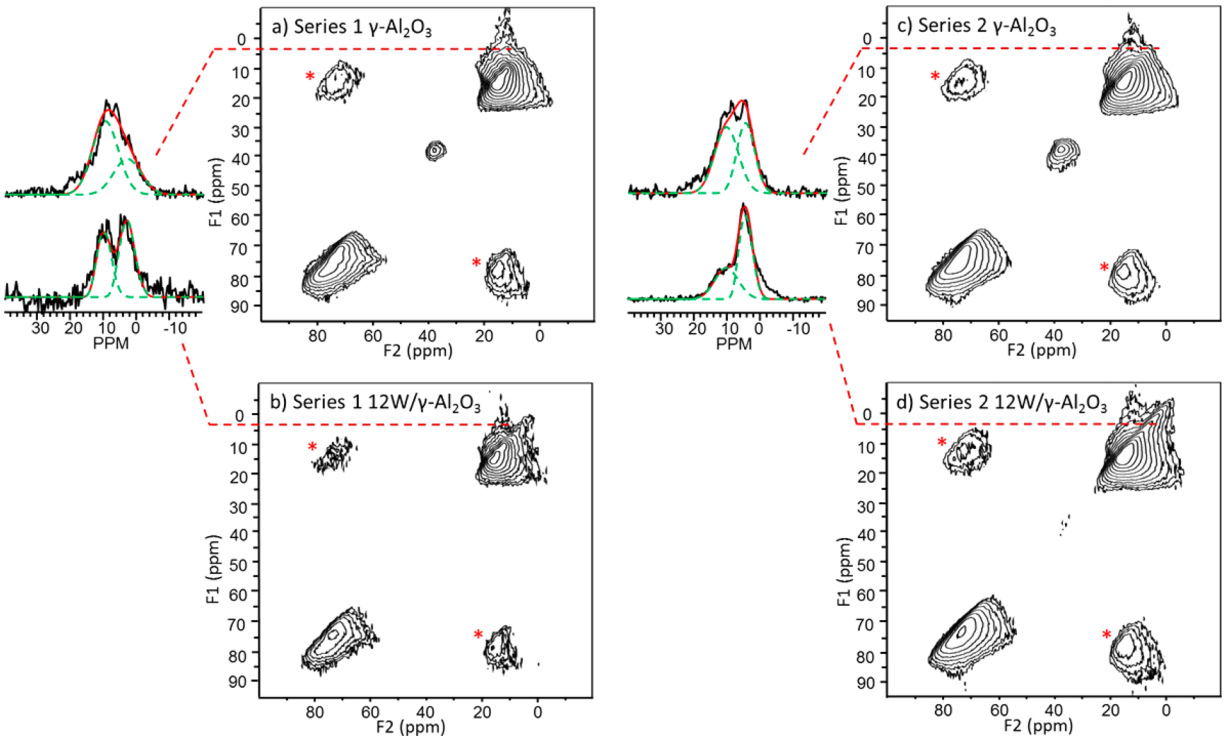

Figure 2. ^{27}Al MQMAS NMR spectra of (a) γ-Al_2O_3 of series 1 with 0 W loading, (b) γ-Al_2O_3 of series 1 with 12 W loading, (c) γ-Al_2O_3 of series 2 with 0 W loading, and (d) γ-Al_2O_3 of series 2 with 12 W loading. For the sliced spectra, the dashed green lines indicate deconvoluted peaks; solid red lines are simulated overall spectra; solid black lines are experimental spectra. The asterisks denote spinning side bands.

NMR spectra, the 1D SP MAS ^{27}Al NMR spectra can be fit quantitatively by locking these key parameters, i.e., allowing less than a 5% variation during fitting. The results from spectral fittings are summarized in Figure 3, while the detailed fitting parameters are summarized in Table S3. Note that the quantity of each Al site extracted from the 1D simulation is normalized to the absolute integrated signal intensity per unit scan and per unit sample weight. As shown in Figure 3, three quadrupolar line shapes are identified in the Al_O region. These correspond to the γ-Al_2O_3 phase with isotropic chemical shift at about 16 ppm,[14,17] Al nucleation sites that eventually evolve into the θ-Al_2O_3 phase (N_θ, near 13 ppm),[46,47] and an additional unassigned alumina phase that appears at the lowest isotropic chemical shift of about 7 ppm (O_{un}-Al_2O_3).[23,46,48] Likewise, for the Al_T spectral region, three unique quadrupolar line shapes are observed that can be related to the N_θ-Al_2O_3 (isotropic chemical shift at about 80 ppm), γ-Al_2O_3 (near 74 ppm), and T_{un}-Al_2O_3 (tetrahedral Al sites that are unassigned around 67 ppm) phases.[14,17,23,46−48] Furthermore, the isotropic chemical shifts of Al_P sites for the two series are located at about 38 ppm.

The results in Figure 4 and Figure S3, where the normalized peak areas for Al_O, Al_T, Al_P, and O_{un}-Al_2O_3 sites as a function of WO_X loading are shown, allow for the Al sites to be compared quantitatively between samples with different WO_X loadings. Since the amount of each type of Al site is proportional to its corresponding integrated peak intensity, the results clearly show that the amount of total Al_P and total Al_O sites changes monotonically with the increasing of WO_X loading. Specifically, the quantity of total Al_O sites and O_{un}-Al_2O_3 sites are shown to increase with greater WO_X loading while the amount of Al_P sites decreases accordingly for both the platelike and the regular Al_2O_3 series. This result strongly indicates that the Al_P sites are the WO_X anchoring positions. Furthermore, the quantity of Al_O sites, especially the detected O_{un}-Al_2O_3 species, increases fast at lower W loadings and approaches a plateau when the Al_P sites are consumed, suggesting the loaded WO_X species prefer to generate new Al_O sites at low W loading, resulting in better dispersion of WO_X species at low loadings. This result is further validated by the relatively unchanged Al_T intensities over the entire WO_X loading values studied, indicating no noticeable correlation between Al_T region and WO_X loading.

To further validate the association of WO_X with the pentahedral Al^{3+} ions, the data points for γ-Al_2O_3 samples at low WO_X loading (i.e., 0, 0.2, 0.5, and 1 W/nm^2 loadings) are analyzed further, and the results are summarized in Figure S4. For series 1, it is obvious (Figure S4a−c) that the peak areas of Al_P and Al_O (both the sum of Al_O sites and the O_{un}-Al_2O_3 site) sites change linearly with increasing WO_X loading (R-squared values: 0.96 for Al_O, 0.81 for Al_P, and 0.93 for O_{un}-Al_2O_3). Meanwhile, the slope values of total Al_O site and O_{un}-Al_2O_3 site (1.0 and 1.4, respectively) are in correlation with the value of Al_P site (−0.9), suggesting that the decreased amount of Al_P sites is almost the same as the increased amount of O_{un}-Al_2O_3 sites at low loading of WO_X on the platelike γ-Al_2O_3 surface (series 1). These results strongly support the conclusion that WO_X interacts with the γ-Al_2O_3 surface by preferentially interacting with Al_P surface sites, and the anchored Al_P sites turn to O_{un}-Al_2O_3 sites. Similarly, the regular series 2 (Figure S4d−f) data demonstrate the same growth and decay trends, but the correlations (R-squared values: 0.54 for Al_O, 0.87 for Al_P, and 0.88 for O_{un}-Al_2O_3) are not as convincing as those obtained from series 1.

To quantitatively determine the dispersion of WO_X on the surface Al_P sites, the number of Al_P sites from the estimated SP NMR peak areas and the known WO_X loading are used to

DOI: 10.1021/acs.jpcc.6b09060
J. Phys. Chem. C 2016, 120, 23093−23103

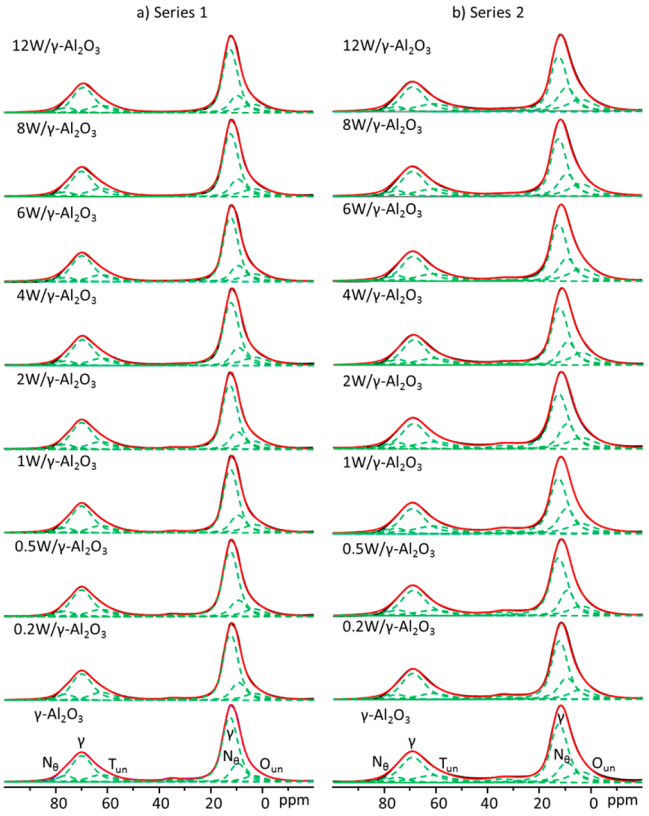

Figure 3. Quadrupolar line shape simulated 1D ^{27}Al MAS NMR spectra of WO_X/γ-Al_2O_3 samples with different WO_X loadings of (a) platelike series 1 and (b) regular series 2. The dashed green lines indicate deconvoluted peaks; solid red lines are simulated overall spectra; solid black lines are experimental spectra. "N_α": Al nucleation sites that eventually evolve into the α-Al_2O_3 phase; "N_θ": Al nucleation sites that eventually evolve into the θ-Al_2O_3 phase; "O_{un}" and "T_{un}": octahedral and tetrahedral Al sites that remain unassigned based on our recent work.[23]

calculate the average number of W per Al_P site in accordance with the following equation:

$$\frac{W}{Al_P\ \text{occupied}} = \frac{\frac{Wt(W)\,\% \times m(\text{sample})}{M(W)}}{\frac{Wt(Al_P\ \text{occupied})\,\% \times m(\text{sample})}{M(Al)}} = \frac{Wt(W)\%}{Wt(Al_P\ \text{occupied})\%} \times \frac{26.98}{183.84}$$

where m is the mass of the sample, M is the molecular weight, and Wt% is the loading in weight percentage. The calculated results are summarized in Table S4. Figure 5 displays the number of W atoms per Al_P sites as a function of WO_X loading on γ-Al_2O_3 surface. Two linear relationships can be defined between the W/Al_P (occupied) and the WO_X loading: one at low (0−1 W/nm^2) loading and the other one at high (2−12 W/nm^2) loading. Comparing these two linear trend lines, the slopes at low W loading (0.4748 for platelike series 1 and 2.5048 for the regular series 2) are significantly higher than those at high loading (0.2657 for series 1 and 0.2979 for series 2). At low loadings, the change in the quantity of tungsten anchored aluminum is much more drastic than at higher tungsten loadings. This possibly suggests that at higher loadings tungsten is forming larger domains that possess more W−O−W bridging structures that anchor to the surface aluminum less

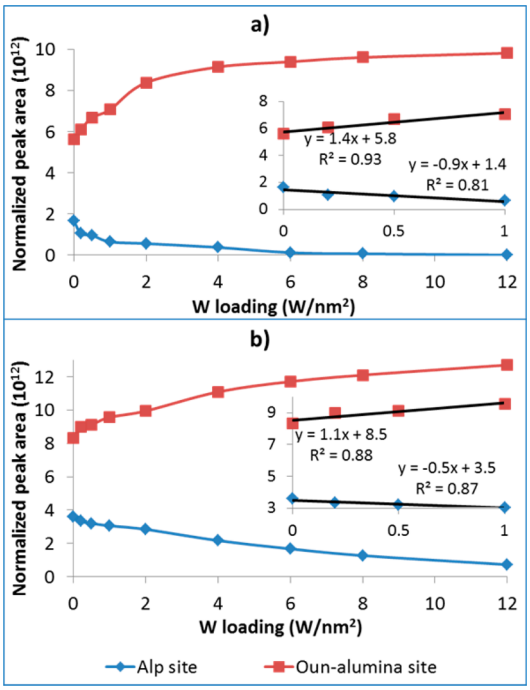

Figure 4. Normalized integrated peak areas of O_{un}-Al_2O_3 and Al_P sites as a function of WO_X loading. (a) O_{un}-Al_2O_3 site and Al_P site of series 1. (b) O_{un}-Al_2O_3 site and Al_P site of series 2. The insets indicate the corresponding linear corrections at low W loading, wherein the black lines are the linear trend lines. The corresponding equations and *R*-squared values displayed.

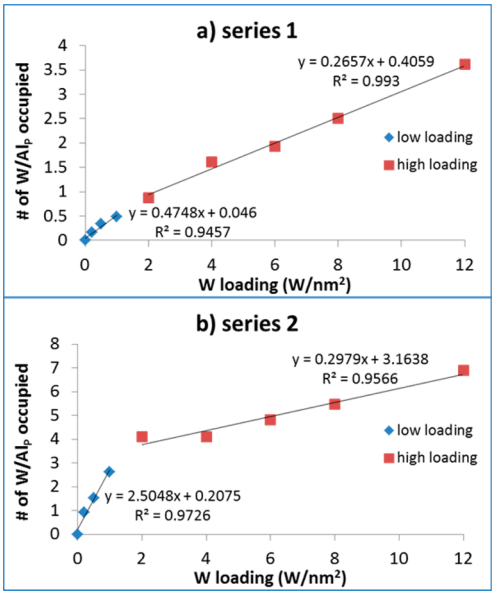

Figure 5. Number of W atoms per Al_P sites as a function of W loading on γ-Al_2O_3 surface: (a) platelike series 1 and (b) regular series 2.

per tungsten atom (e.g., trimers). This may be due to fewer new Al_P sites being available at higher loadings where the plateau region is prevalent (see Figure 4). Additionally, the W/Al_P (occupied) value of 2 W/nm^2 loading for series 1 (0.88) and 0.2 W/nm^2 loading for series 2 (0.92) are less than 1, suggesting that each occupied Al_P site interacts with no more than one tungsten atom and thus meaning the loaded WO_X must be atomically dispersed on the occupied Al_P sites at low W loading (2 W/nm^2 and lower for series 1 and 0.2 W/nm^2

DOI: 10.1021/acs.jpcc.6b09060
J. Phys. Chem. C 2016, 120, 23093−23103

and lower for series 2), and larger WO_X domains are formed as monolayer coverage is approached.[49] Furthermore, by the comparison between the trend lines of the low loading samples for the two different series, the slope of series 1 (0.4748) is obviously lower than that of series 2 (2.5048), indicating the loading of tungsten for each Al_P sites of series 1 is less than that of series 2 as can be also seen directly in the occupation values; i.e., the dispersion of loaded WO_X on series 1 γ-Al_2O_3 is higher than that on series 2 γ-Al_2O_3. Also, as shown in Table S4, the Al_P sites per nm^2 of the bare series 1 γ-Al_2O_3 (3.32 Al_P/nm^2) is higher than that of series 2 (2.12 Al_P/nm^2), suggesting higher density of Al_P sites for the series 1 catalyst support. These results strongly imply that better dispersion and a greater quantity of Al_P sites are obtained for the platelike series 1 γ-Al_2O_3, making it a better catalyst support than regular series 2.

In summary, the following results are obtained. (1) WO_X interacts with alumina by preferentially anchoring to the Al_P Al^{3+} surface sites at low metal loading. (2) With the loading of WO_X in γ-Al_2O_3 surface, the Al_P site turns into the O_{un}-Al_2O_3 site in the ^{27}Al MAS NMR spectra. (3) The loaded WO_X is atomically dispersed on the occupied Al_P sites at low W loading ($\leqslant$2 W/nm^2 for series 1 and $\leqslant$0.2 W/nm^2 for series 2), and larger WO_X domains are formed at higher W loading situation. (4) The platelike series 1 γ-Al_2O_3 is a more suitable catalyst support than series 2.

3.4. $^1H-^{27}Al$ CP NMR. Figure 6 shows the comparison between 1D SP ^{27}Al MAS and $^1H-^{27}Al$ CP MAS NMR spectra.

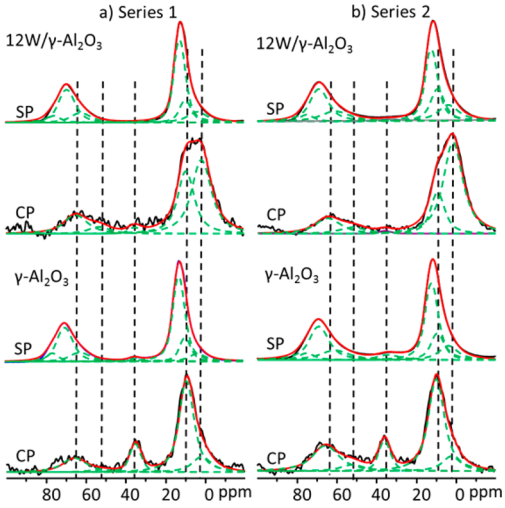

Figure 6. SP ^{27}Al MAS NMR and $^1H-^{27}Al$ CP NMR spectra of γ-Al_2O_3 samples without and with WO_X loading. (a) Platelike series 1. (b) Regular series 2. The dashed green lines indicate deconvoluted peaks; solid red lines are simulated overall spectra; solid black lines are experimental spectra.

The CP MAS NMR spectra emphasize the signal contributions from the surface where only Al sites that are close to surface protons (−OH groups) are observed. Since Al_p sites are exclusively surface species, the peak corresponding to the Al_P sites in the CP MAS NMR spectra is dramatically enhanced compared with its counterpart in the SP MAS NMR spectra. Another very interesting finding is that for both the Al_O and the Al_T spectral regions the peak center is shifted upfield dramatically in the CP MAS NMR spectra compared with that of the SP spectra, possibly due to aluminum's proximity to hydroxyl groups or water. A detailed evaluation of the deconvoluted peaks reveals that the peaks corresponding to the O_{un}-Al_2O_3 sites are also dramatically enhanced in the CP MAS spectra. Like the results obtained from 1D SP ^{27}Al MAS NMR above, the intensities of CP Al_P peaks decrease with an increase in WO_X loading for both two series. Meanwhile, the line width of Al_O sites increase significantly with the increasing of WO_X coverage. To obtain more detailed information from the CP spectral results, these spectra can be simulated using the quadrupolar coupling constants derived from the 1D spectra. Two peaks were found at the Al_T and Al_O region, and one peak was used to fit the Al_P region. Figure 6 also displays the simulation lines, and the parameters of simulations are summarized in Table S5.

Obviously, the relative intensity of the most upfield peak, which has isotropic chemical shift at around 5 ppm, dramatically increases with the increasing of WO_X loading. This peak is assigned to O_{un} site of 1D spectra (around 7 ppm). Meanwhile, the relative intensities for the 13 ppm (assigned to N_θ site of Al_O region) and 39 ppm (which is corresponding with Al_P site) peaks decrease with an increasing WO_X loading for both series. Furthermore, there are two peaks at Al_T region: one of the peaks is located at around 70 ppm, which is close to T_{un} site of 1D spectra (around 68 ppm); while another small peak is located at around 57 ppm, which is not observed in the corresponding 1D spectra. These results suggest that (1) most of the Al_P and unassigned (T_{un} and O_{un}) sites are dispersed at the γ-Al_2O_3 surface and (2) the conclusion of WO_X transforming the surface Al_P sites to O_{un}-Al_2O_3 sites is further validated.

3.5. DFT Simulations. *3.5.1. Computational Modeling and the Calculated NMR Parameters for γ-Al_2O_3 without WO_X Loadings.* Based on previous studies, the predominant terminations of γ-Al_2O_3 surface are the (110) (74% abundance), (100) (16% abundance), and (111) (10% abundance) facets.[30,50−52] It has also been reported that the (100) facet is the preferentially interacted surface for anchored metal oxides because of its relatively low hydration state compared with the low reactivity of the (110)[6,53−55] and the (111)[29,30] facets under the pretreatment conditions of 450 °C in flowing dry air. Therefore, we focus our investigations of the bare γ-Al_2O_3 surface on the most reactive (100) facet and the most abundance (110) facet and WO_X anchored γ-Al_2O_3 surface on the most reactive (100) facet. Before calculations of WO_X/γ-Al_2O_3 clusters, the γ-Al_2O_3 surfaces of the (100) and (110) facets were constructed first. The periodic model published by Krokidi et al.,[28] derived from simulating the dehydration process of the boehmite precursor, was used as the base model for constructing the cluster models for the DFT surface calculations herein. Note that with this approach the terminal oxygen atoms were charge balanced by adding hydrogen atoms. Both the (100) and (110) surfaces were simulated using both fully dehydrated and hydrated models. The geometrically optimized models were used to calculate the corresponding NMR parameters, including chemical shift and C_Q. For the model of (100) facet, five central pentahedral coordinated surface Al sites were selected for comparing the changes of NMR parameters, while for the model of (110) facet, four central pentahedral and one trihedral surface Al sites were selected (see Figure S5). The calculated NMR parameters for surface sites of all terminations are summarized in Table S6.

Figure 7a shows the distribution of calculated chemical shifts and C_Q values for the various Al sites on bare γ-Al_2O_3 surface, which clearly demonstrate clustering into four groups based on

DOI: 10.1021/acs.jpcc.6b09060
J. Phys. Chem. C 2016, 120, 23093−23103

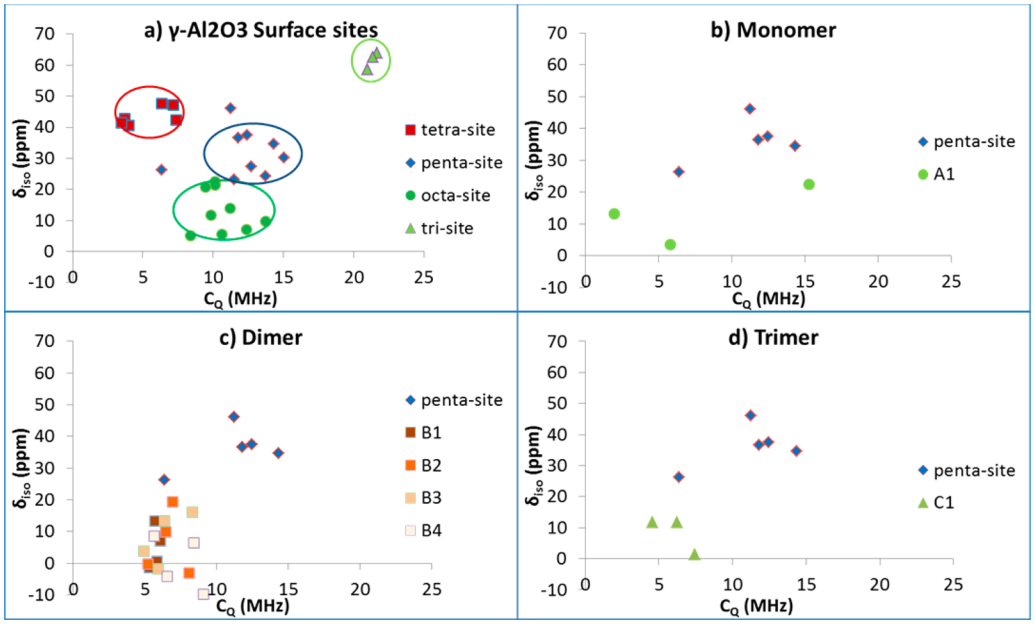

Figure 7. (a) Calculated isotropic chemical shift (δ_{iso}) as a function of C_Q for Al surface sites on (100) and (110) terminations of γ-Al_2O_3 at various levels of hydration. Calculated δ_{iso} as a function of C_Q for pentacoordinated Al surface sites on (100) terminations of γ-Al_2O_3 that are anchored by (b) monomer WO_X cluster, (c) dimer WO_X cluster, and (d) trimer WO_X cluster, where detailed models corresponding to **A1**, **B1**−**B4**, and **C1** are given in Table 1. The 3-coordinated γ-Al_2O_3 sites have δ_{iso} values of 60−70 ppm and C_Q values of 20−25 MHz. The tetracoordinated Al sites have δ_{iso} values of 40−50 ppm and C_Q values of 3−8 MHz. The pentacoordinated have δ_{iso} values of 25−40 ppm and C_Q values of 10−15 MHz, while the octahedral Al sites have δ_{iso} value of 0−25 ppm and C_Q of 7−12 MHz.

the type of Al coordination. The calculated chemical shifts values for Al_O (0−25 ppm) and Al_P (25−40 ppm) sites are in good agreement with the corresponding experimental values (0−20 and 38 ppm, respectively), indicating the validity of the models. However, the calculated values of Al_T (40−50 ppm) are smaller than the experimental values (60−80 ppm) primarily due to the use of cluster models where the Al_T sites are all on the surface or close to the surface and Al_P sites. Note that the chemical shift (60−80 ppm) for Al_T are obtained from the quantitative 1D ^{27}Al MAS NMR spectra where the bulk Al_T species dominate. Therefore, the calculated 40−50 ppm chemical shifts for the Al_T are likely due to those sites that are near the surface, considering a 57 ppm peak was observed from the spectral simulation results of the surface-sensitive ^{1}H−^{27}Al CP NMR spectra (see section 3.4 and Figure 6, Table S5). Furthermore, the resulting distribution of the calculated C_Q values for Al_T and Al_O sites conforms to experimental results (around 5 MHz for Al_T site and around 6 MHz for Al_O site from the line fitting results of 1D experimental spectra). It is also observed that the predicted C_Q values for the Al_P sites (10−15 MHz) are higher than the experimental results (around 6 MHz), indicating the Al_P sites experience significant dynamics such as bond vibrations. It is generally accepted in the field of NMR that molecular motion can partially average the anisotropic line shape to generate a narrowed peak depending on the degree of the motion or dynamics. Therefore, these surface models are consistent with experimental results and are suitable for the further investigation on the effects of WO_X anchoring.

3.5.2. Effect of WO_X Anchoring on the Surface Sites to the NMR Parameters. After successfully constructing the bare surface structures of γ-Al_2O_3, WO_X clusters were anchored onto the surface sites of (100) facet. The NMR chemical shifts were calculated on fully optimized models, and the results are summarized in Table 1 and Table S7. Figures 7b−d highlight the distribution of calculated chemical shifts and C_Q for WO_X anchored Al_P sites, showing that monomers, dimers, and trimmers exhibit quadrupolar coupling constants akin to those

Table 1. Calculated ^{27}Al Averaged Chemical Shifts in Ppm of WO_X Loaded Al_P Sites with α-Al_2O_3 Cluster as a Secondary Reference to $Al(NO_3)_3$ (0 ppm)

Model surface W-species after geometry optimization[a]	Structure label	WO_X cluster formula	Averaged calculated ^{27}Al NMR chemical shifts (ppm) with WO_X loading	Averaged calculated ^{27}Al NMR chemical shifts (ppm) without WO_X loading
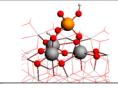	A1	WO_5H_2	13	36
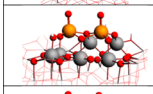	B1	$W_2O_8H_1$	5	39
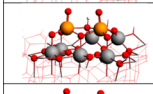	B2	$W_2O_8H_1$	6	39
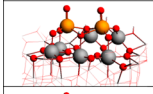	B3	$W_2O_8H_1$	8	39
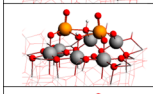	B4	$W_2O_8H_2$	0	39
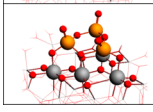	C1	W_3O_9	8	32

[a]The atoms that are not directly connected to a WO_X cluster display as wireframe. Color scheme: yellow, tungsten (W); gray, aluminum (Al); red, oxygen (O); white, hydrogen (H).

DOI: 10.1021/acs.jpcc.6b09060
J. Phys. Chem. C 2016, 120, 23093−23103

reported for octahedral sites; detailed parameters are summarized in Table S8.

Four monomeric tungsten species were examined for the (100) facet. Most notable is a W-cluster model with formula of WO_5H_2 (labels as **A1** in Table 1) has one double bond with oxygen, one single bond connected to an −OH group, and three W−O−Al bonds anchored to the three oxygen atoms belonging to three different Al_P sites. The predicted chemical shift value of **A1** for the Al_P sites with WO_X anchored is decreased from the corresponding bare Al_P sites of 36 ppm to the anchored sites of 13 ppm, which is close to the experimental isotropic chemical shift of O_{un}-Al_2O_3 sites (about 7 ppm). **A1** is a highly probable morphology given that the experimental isotropic chemical shift of Al_P sites (about 38 ppm) migrates to the upfield edge of the Al_O position to about 7 ppm. Detailed information and discussion regarding the calculations of the three additionally nonpreferential monomeric WO_X anchored structural models (**A2**, **A3**, and **A4**) are provided in the Supporting Information Section S1 and Table S7. Therefore, the VI valent WO_X species, **A1**, is likely the preferential monomeric anchored mode.

Dimeric tungsten species allow for the consideration of several morphological possibilities. Initially, we tried the structures with two W−O−W bridges, and the geometry optimization successfully converged. These clusters are labeled as **B1**, **B2**, **B3**, and **B4** in Table 1 as well as **B5** and **B6** in Table S7. In each of the first four dimeric models (**B1**, **B2**, **B3**, and **B4**), each W atom has one double-bond oxygen atom and four single-bond oxygen atoms where two of them are W−O−Al bonds and two are W−O−W bridges. To consider the role of Brønsted acid location on supported tungsten oxide catalysts,[56−62] the placement of acidic −OH groups was investigated for these structures, either in W−OH^+−W or W−OH^+−Al acidic form. The structure in **B1** has one acidic hydrogen on one of the W−O−Al bonds, giving rise to a calculated ^{27}Al isotropic chemical shift value of 5 ppm for the W-anchored Al_P sites. Likewise, the structures in both **B2** (6 ppm) and **B3** (8 ppm) have one acidic hydrogen on one of the two W−O−W bridges giving rise to calculated ^{27}Al isotropic chemical shift values of 6 ppm (**B2**) and 8 ppm (**B3**) for the W-anchored Al_P sites, respectively, and **B4** with 0 ppm for the anchored Al_P sites has two acidic hydrogen on both the two bridging W−O−W bonds. Clearly, with the increasing number of Brønsted acidic hydrogens, the averaged isotropic chemical shift value for the anchored Al sites decreases. Even though these dimeric structural models slightly differ from each other, the predicted isotropic chemical shifts for the anchored penta-Al sites are all in excellent agreement with the experimental results.

Additional double W−O−W bridge structures were considered in models **B5** and **B6** (see Table S7). The frames of the WO_X cluster are asymmetric, where one of the tungsten atoms of **B5** has one W−O−Al bond and one of the tungsten atoms of **B6** has no double-bond oxygen atom. The structure **B5** has no acidic hydrogen, giving rise to a predicted ^{27}Al isotropic chemical shift value of 10 ppm for the anchored Al_P sites. Furthermore, the structure **B6** has two acidic hydrogen atoms on both bridging W−O−W bonds, giving rise to a predicted chemical shift of 11 ppm for the anchored sites. Thus, these two asymmetric structures are close to the experimental results since the experimental isotropic chemical shift of O_{un}-Al_2O_3 sites is about 7 ppm. Detailed information and discussion regarding the calculations of the two additionally non-preferential dimeric WO_X anchored structural models (**B7** and **B8**) are provided in the Supporting Information Section S1 and Table S7.

The trimeric WO_X cluster (W_3O_9), previously studied,[63,64] was evaluated with two different anchoring modes (**C1** in Table 1 and **C2** in Table S7), and their geometry optimizations were successfully converged, indicating stable structures. The parent structure of tungsten oxide has been constructed as a 6-member ring, including three W atoms with two doubly bonded O atoms and three bridging O atoms (see Table S7). In the first trimeric model (C1), all three W atoms are anchored on the surface Al_P sites via a W−O−Al bond. The averaged calculated chemical shift of **C1** is 8 ppm, which is in good agreement with the experimental results (7 ppm). Evaluating the **C2** structure (see Table S7), the top W atom kept its two double-bonded oxygen atoms, and the four bonded O atoms of the two lower W atoms were connected with surface Al_P sites by W−O−Al bonds. However, the averaged predicted chemical shift values (33 ppm) for the anchored Al_P sites in **C2** are close to the value of bare Al_P sites in **C2** (i.e., 40 ppm in Table S7), indicating the unlikely existence of a **C2** structure.

For the predicted C_Q values of the WO_X anchored Al_P sites, most of them have changed from 10 to 15 MHz at bare Al_P sites to 5−10 MHz (see Figure 7b−d), which is consistent with the predicted C_Q values of Al_O sites of bare γ-Al_2O_3 terminations (7−12 MHz, see Figure 7a) as well as the experimental C_Q values of O_{un}-Al_2O_3 site (around 5 MHz, see Table S3). For the Al_T sites of these preferential WO_X anchored (100) facet of γ-Al_2O_3 clusters, most of them presented slightly higher chemical shifts at 50−60 ppm than that of the bare surface (see Figure S6 and Table S9), which is more close to the chemical shift value of the surface Al_T sites from CP spectra (57 ppm, see Figure 6 and Table S5), further validating the consistence between the calculated and experimental results.

In summary, there are several potential anchored WO_X clusters on (100) termination of γ-Al_2O_3. For the monomeric WO_X species, only an −OH group included VI valent WO_X species (i.e., **A1**) generates an isotropic ^{27}Al NMR chemical shift that is close to the experimental result. For the dimeric WO_X species, the acid site location and quantity have an influence on the predicted chemical shifts. Most of the structures (**B1** to **B6**) are in good agreement with the experimental results. For the trimeric WO_X species, only flat anchored trimeric W_3O_9 ring (**C1**) is in agreement with the experimental results.

4. CONCLUSIONS

The γ-Al_2O_3 supported WO_X (WO_X/γ-Al_2O_3) catalysts were used for investigating the metal−support interaction. Two types of γ-Al_2O_3, platelike Al_2O_3 with a surface area of 56.9 m^2/g and regular Al_2O_3 with a surface area of 217.6 m^2/g, were impregnated with a varying amount tungsten oxide (WO_X). Quantitative single pulse ^{27}Al MAS NMR and MQMAS ^{27}Al NMR were conducted to provide both the bulk and the surface information on alumina without discrimination while the surface-sensitive ^{1}H−^{27}Al CP MAS NMR was carried out to obtain information on the local environment of surface Al species. Electronic structural calculations of the ^{27}Al chemical shifts using DFT were used to accurately assign the NMR signals and relate the experimental results to the detailed interactions between tungsten and alumina. The integrated NMR spectroscopy approach allows the observation of at least seven different Al sites, including a penta-Al site with isotropic

DOI: 10.1021/acs.jpcc.6b09060
J. Phys. Chem. C 2016, 120, 23093−23103

chemical shift value located at about 38 ppm, three different tetrahedral Al sites (isotropic chemical shift values at about 79, 74, and 66 ppm), and three octahedral Al sites (isotropic chemical shift values at about 16, 13, and 7 ppm). It is found that the amount of pentacoordinated Al sites decreases monotonically while the amount of octahedral Al (Al_O) sites increases with an increasing WO_X loading, indicating that the Al_p sites are the preferred surface anchoring sites for the WO_X species. For the first time, we found that the Al_P sites with isotropic chemical shift originally located at about 38 ppm observed for the unsupported γ-Al_2O_3 migrates into the octahedral region with new isotropic chemical shift value appearing at about 7 ppm when the Al_p site is anchored by WO_X species. DFT computational modeling of the NMR parameters on proposed cluster models is carried out to accurately interpret the changes of such dramatic chemical shifts from which the detailed anchoring mechanisms are obtained. It is found that tungsten dimers and monomers are the preferred supported surface species on γ-Al_2O_3, wherein one monomeric (**A1** in Table 1) and several dimeric structures (**B1** to **B4** in Table 1 and **B5**, **B6** in Table S7) are identified as the most likely surface anchoring structures.

■ ASSOCIATED CONTENT

Supporting Information

The Supporting Information is available free of charge on the ACS Publications website at DOI: 10.1021/acs.jpcc.6b09060.

Additional discussions of nonpreferential W-loaded γ-Al_2O_3 surface structure; detailed information on samples, fitting parameters of SP, MQMAS, and CP NMR spectra, calculation of W atoms per Al_p sites, calculated NMR parameters and optimized geometries for the calculated models (Table S10); optimized structures of reference clusters and surface structures of γ-Al_2O_3; detailed fitting slices of MQMAS NMR spectra; and detailed peak areas of SP NMR spectra as a function of WO_X loading (PDF)

■ AUTHOR INFORMATION

Corresponding Author

*(J.Z.H.) E-mail Jianzhi.Hu@pnnl.gov; Ph (509) 371-6544; Fax (509) 371-6546 (J.Z.H.).

Notes

The authors declare no competing financial interest.

■ ACKNOWLEDGMENTS

This research was supported by the U.S. Department of Energy (DOE), Office of Basic Energy Sciences, Division of Chemical Sciences, Biosciences and Geosciences (DE-AC05-RL01830, FWP-47319). All of the NMR experiments were performed in the Environmental Molecular Sciences Laboratory, a national scientific user facility sponsored by the DOE's Office of Biological and Environmental Research, and located at Pacific Northwest National Laboratory (PNNL). PNNL is a multi-program national laboratory operated for the DOE by Battelle Memorial Institute under Contract DE-AC06-76RLO 1830.

■ REFERENCES

(1) Hudson, L. K.; Misra, C.; Perrotta, A. J.; Wefers, K.; Williams, F. S. Aluminum Oxide. In *Ullmann's Encyclopedia of Industrial Chemistry*; Wiley-VCH Verlag GmbH & Co. KGaA: 2000; Vol. 2, pp 507–644.

(2) Trueba, M.; Trasatti, S. P. γ-Alumina as a Support for Catalysts: A review of Fundamental Aspects. *Eur. J. Inorg. Chem.* **2005**, *2005*, 3393–3403.

(3) Voss, G. J. B.; Chavez Panduro, E. A.; Midttveit, A.; Fløystad, J. B.; Høydalsvik, K.; Gibaud, A.; Breiby, D. W.; Rønning, M. Mesostructured Alumina as Powders and Thin Films. *J. Mater. Chem. A* **2014**, *2*, 9727.

(4) Alonso-Fagundez, N.; Granados, M. L.; Mariscal, R.; Ojeda, M. Selective conversion of furfural to maleic anhydride and furan with VO_X/Al_2O_3 catalysts. *ChemSusChem* **2012**, *5*, 1984–90.

(5) Busca, G. The Surface of Transitional Aluminas: A Critical Review. *Catal. Today* **2014**, *226*, 2–13.

(6) Wischert, R.; Laurent, P.; Coperet, C.; Delbecq, F.; Sautet, P. γ-Alumina: the Essential and Unexpected Role of Water for the Structure, Stability, and Reactivity of "Defect" Sites. *J. Am. Chem. Soc.* **2012**, *134*, 14430–14449.

(7) O'Neill, B. J.; Sener, C.; Jackson, D. H.; Kuech, T. F.; Dumesic, J. A. Control of Thickness and Chemical Properties of Atomic Layer Deposition Overcoats for Stabilizing Cu/γ-Al_2O_3 Catalysts. *ChemSusChem* **2014**, *7*, 3247–51.

(8) Lwin, S.; Wachs, I. E. Olefin Metathesis by Supported Metal Oxide Catalysts. *ACS Catal.* **2014**, *4*, 2505–2520.

(9) Deng, H.; Yu, Y.; He, H. Discerning the Role of Ag–O–Al Entities on Ag/γ-Al_2O_3 Surface in NOx Selective Reduction by Ethanol. *J. Phys. Chem. C* **2015**, *119*, 3132–3142.

(10) Zhang, Z.; Hicks, R. W.; Pauly, T. R.; Pinnavaia, T. J. Mesostructured Forms of γ-Al_2O_3. *J. Am. Chem. Soc.* **2002**, *124*, 1592–1593.

(11) Tsyganenko, A. A.; Mardilovich, P. P. Structure of Alumina Surfaces. *J. Chem. Soc., Faraday Trans.* **1996**, *92*, 4843–4852.

(12) Pecharromán, C.; Sobrados, I.; Iglesias, J. E.; González-Carreño, T.; Sanz, J. Thermal Evolution of Transitional Aluminas Followed by NMR and IR Spectroscopies. *J. Phys. Chem. B* **1999**, *103*, 6160–6170.

(13) Carrier, X.; d'Espinose de la Caillerie, J.-B.; Lambert, J.-F.; Che, M. The Support as a Chemical Reagent in the Preparation of WOx/γ-Al_2O_3 Catalysts: Formation and Deposition of Aluminotungstic Heteropolyanions. *J. Am. Chem. Soc.* **1999**, *121*, 3377–3381.

(14) Kwak, J. H.; Hu, J.; Mei, D.; Yi, C. W.; Kim, D. H.; Peden, C. H. F.; Allard, L. F.; Szanyi, J. Coordinatively Unsaturated Al^{3+} Centers as Binding Sites for Active Catalyst Phases of Platinum on γ-Al_2O_3. *Science* **2009**, *325*, 1670–1673.

(15) Ferreira, A. R.; Küçükbenli, E. K.; Leitão, A. A.; de Gironcoli, S. Ab Initio ^{27}Al NMR Chemical Shifts and Quadrupolar Parameters for Al_2O_3 Phases and Their Precursors. *Phys. Rev. B: Condens. Matter Mater. Phys.* **2011**, *84*, 235119.

(16) Ravenelle, R. M.; Copeland, J. R.; Kim, W.-G.; Crittenden, J. C.; Sievers, C. Structural Changes of γ-Al_2O_3-Supported Catalysts in Hot Liquid Water. *ACS Catal.* **2011**, *1*, 552–561.

(17) Düvel, A.; Romanova, E.; Sharifi, M.; Freude, D.; Wark, M.; Heitjans, P.; Wilkening, M. Mechanically Induced Phase Transformation of γ-Al_2O_3 into α-Al_2O_3. Access to Structurally Disordered γ-Al_2O_3 with a Controllable Amount of Pentacoordinated Al Sites. *J. Phys. Chem. C* **2011**, *115*, 22770–22780.

(18) Kwak, J. H.; Hu, J. Z.; Kim, D. H.; Szanyi, J.; Peden, C. H. F. Penta-Coordinated Al^{3+} Ions as Preferential Nucleation Sites for BaO on γ-Al_2O_3: An Ultra-High-Magnetic Field ^{27}Al MAS NMR Study. *J. Catal.* **2007**, *251*, 189–194.

(19) Fu, L.; Li, X.; Liu, M.; Yang, H. Insights into the Nature of Cu Doping in Amorphous Mesoporous Alumina. *J. Mater. Chem. A* **2013**, *1*, 14592.

(20) Kim, J. M.; Kwak, J. H.; Jun, S.; Ryoo, R. Ion Exchange and Thermal Stability of MCM-41. *J. Phys. Chem.* **1995**, *99*, 16742–16747.

(21) Cho, I. H.; Park, S. B.; Kwak, J. H. Characterization of $MoAl_2O_3$ Sol-Gel Catalyst by ^{27}Al Nuclear Magnetic Resonance Spectroscopy. *J. Mol. Catal. A: Chem.* **1996**, *104*, 285–291.

(22) Liu, X.; Truitt, R. E. DRFT-IR Studies of the Surface of γ-Alumina. *J. Am. Chem. Soc.* **1997**, *119*, 9856–9860.

(23) Hu, J. Z.; Xu, S.; Kwak, J. H.; Hu, M. Y.; Wan, C.; Zhao, Z.; Szanyi, J.; Bao, X.; Han, X.; Wang, Y.; et al. High Field ^{27}Al MAS NMR

DOI: 10.1021/acs.jpcc.6b09060
J. Phys. Chem. C 2016, 120, 23093–23103

and TPD Studies of Active Sites in Ethanol Dehydration Using Thermally Treated Transitional Aluminas as Catalysts. *J. Catal.* **2016**, *336*, 85−93.
(24) Sarou-Kanian, V.; Gleizes, A. N.; Florian, P.; Samélor, D.; Massiot, D.; Vahlas, C. Temperature-Dependent 4-, 5- and 6-Fold Coordination of Aluminum in MOCVD-Grown Amorphous Alumina Films: A Very High Field ^{27}Al-NMR study. *J. Phys. Chem. C* **2013**, *117*, 21965−21971.
(25) Wischert, R.; Florian, P.; Coperet, C.; Massiot, D.; Sautet, P. Visibility of Al Surface Sites of γ-Alumina: A Combined Computational and Experimental Point of View. *J. Phys. Chem. C* **2014**, *118*, 15292−15299.
(26) Park, J.-W.; Thomas, K.; van Gestel, J.; Gilson, J.-P.; Collet, C.; Dath, J.-P.; Houalla, M. Study of Ir/WO_3/Al_2O_3 Ring Opening Catalysts. *Appl. Catal., A* **2010**, *388*, 37−44.
(27) Liu, C.; Zhang, C.; Sun, S.; Liu, K.; Hao, S.; Xu, J.; Zhu, Y.; Li, Y. Effect of WOx on Bifunctional Pd−WOx/Al_2O_3 Catalysts for the Selective Hydrogenolysis of Glucose to 1,2-Propanediol. *ACS Catal.* **2015**, *5*, 4612−4623.
(28) Krokidis, X.; Raybaud, P.; Gobichon, A.-E.; Rebours, B.; Euzen, P.; Toulhoat, H. Theoretical Study of the Dehydration Process of Boehmite to γ-Alumina. *J. Phys. Chem. B* **2001**, *105*, 5121−5130.
(29) Digne, M.; Sautet, P.; Raybaud, P.; Euzen, P.; Toulhoat, H. Hydroxyl Groups on Gamma-Alumina Surfaces: A DFT Study. *J. Catal.* **2002**, *211*, 1−5.
(30) Digne, M.; Sautet, P.; Raybaud, P.; Euzen, P.; Toulhoat, H. Use of DFT to Achieve a Rational Understanding of Acid-Basic Properties of γ-Alumina Surfaces. *J. Catal.* **2004**, *226*, 54−68.
(31) Joubert, J.; Delbecq, F.; Sautet, P.; Le Roux, E.; Taoufik, M.; Thieuleux, C.; Blanc, F.; Coperet, C.; Thivolle-Cazat, J.; Basset, J. M. Molecular Understanding of Alumina Supported Single-Site Catalysts by a Combination of Experiment and Theory. *J. Am. Chem. Soc.* **2006**, *128*, 9157−9169.
(32) Digne, M.; Raybaud, P.; Sautet, P.; Guillaume, D.; Toulhoat, H. Quantum Chemical and Vibrational Investigation of Sodium Exchanged γ-Alumina Surfaces. *Phys. Chem. Chem. Phys.* **2007**, *9*, 2577−2582.
(33) Liźarraga, R.; Holmström, E.; Parker, S. C.; Arrouvel, C. Structural Characterization of Amorphous Alumina and Its Polymorphs from First-Principles XPS and NMR Calculations. *Phys. Rev. B: Condens. Matter Mater. Phys.* **2011**, *83*, 094201.
(34) Peintinger, M. F.; Kratz, M. J.; Bredow, T. Quantum-Chemical Study of Stable, Meta-Stable and High-Pressure Alumina Polymorphs and Aluminum Hydroxides. *J. Mater. Chem. A* **2014**, *2*, 13143.
(35) Medek, A.; Harwood, J. S.; Frydman, L. Multiple-Quantum Magic-Angle Spinning NMR: A New Method for the Study of Quadrupolar Nuclei in Solids. *J. Am. Chem. Soc.* **1995**, *117*, 12779−12787.
(36) Amoureux, J. P.; Fernandez, C.; Steuernagel, S. ZFiltering in MQMAS NMR. *J. Magn. Reson., Ser. A* **1996**, *123*, 116−118.
(37) Metz, G.; Wu, X. L.; Smith, S. O. Ramped-Amplitude Cross Polarization in Magic-Angle-Spinning NMR. *J. Magn. Reson., Ser. A* **1994**, *110*, 219−227.
(38) Massiot, D.; Fayon, F.; Capron, M.; King, I.; Le Calve, S.; Alonso, B.; Durand, J. O.; Bujoli, B.; Gan, Z. H.; Hoatson, G. Modelling One- and Two-Dimensional Solid-State NMR Spectra. *Magn. Reson. Chem.* **2002**, *40*, 70−76.
(39) Grimme, S.; Antony, J.; Schwabe, T.; Muck-Lichtenfeld, C. Density Functional Theory with Dispersion Corrections for Supramolecular Structures, Aggregates, and Complexes of (bio)Organic Molecules. *Org. Biomol. Chem.* **2007**, *5*, 741−58.
(40) Van Lenthe, E.; Baerends, E. J. Optimized Slater-Type Basis Sets for the Elements 1−118. *J. Comput. Chem.* **2003**, *24*, 1142−56.
(41) Schreckenbach, G.; Ziegler, T. The Calculation of NMR Shielding Tensors Based on Density Functional Theory and the Frozen-Core Approximation. *Int. J. Quantum Chem.* **1996**, *60*, 753−766.
(42) Schreckenbach, G.; Ziegler, T. Density Functional Calculations of NMR Chemical Shifts and ESR g-tensors. *Theor. Chem. Acc.* **1998**, *99*, 71−82.
(43) Alkan, F.; Dybowski, C. Calculation of Chemical-Shift Tensors of Heavy Nuclei: a DFT/ZORA Investigation of ^{199}Hg Chemical-Shift Tensors in Solids, and the Effects of Cluster Size and Electronic-State Approximations. *Phys. Chem. Chem. Phys.* **2014**, *16*, 14298−308.
(44) Lewis, J.; Schwarzenbach, D.; Flack, H. D. Electric Field Gradients and Charge Density in Corundum, α-Al_2O_3. *Acta Crystallogr., Sect. A: Cryst. Phys., Diffr., Theor. Gen. Crystallogr.* **1982**, *38*, 733−739.
(45) Zhao, Z.; Xu, S.; Hu, M. Y.; Bao, X.; Peden, C. H. F.; Hu, J. Investigation of Aluminum Site Changes of Dehydrated Zeolite H-Beta during a Rehydration Process by High-Field Solid-State NMR. *J. Phys. Chem. C* **2015**, *119*, 1410−1417.
(46) Kovarik, L.; Bowden, M.; Shi, D.; Washton, N. M.; Andersen, A.; Hu, J. Z.; Lee, J.; Szanyi, J.; Kwak, J.-H.; Peden, C. H. F. Unraveling the Origin of Structural Disorder in High Temperature Transition Al_2O_3: Structure of θ-Al_2O_3. *Chem. Mater.* **2015**, *27*, 7042−7049.
(47) O'Dell, L. A.; Savin, S. L. P.; Chadwick, A. V.; Smith, M. E. A Al-27 MAS NMR Study of a Sol-Gel Produced Alumina: Identification of the NMR Parameters of the Theta-Al_2O_3 Transition Alumina Phase. *Solid State Nucl. Magn. Reson.* **2007**, *31*, 169−173.
(48) Kovarik, L.; Bowden, M.; Genc, A.; Szanyi, J.; Peden, C. H. F.; Kwak, J. H. Structure of δ-Alumina: Toward the Atomic Level Understanding of Transition Alumina Phases. *J. Phys. Chem. C* **2014**, *118*, 18051−18058.
(49) Soled, S.; Murrell, L. L.; Wachs, I. E.; McVicker, G. B.; Sherman, L. G.; Chan, S.; Dispenziere, N. C.; Baker, R. T. K. Solid State Chemistry of Tungsten Oxide Supported on Alumina. *ACS Symp. Ser.* **1985**, *279*, 165−182.
(50) Gribov, E. N.; Zavorotynska, O.; Agostini, G.; Vitillo, J. G.; Ricchiardi, G.; Spoto, G.; Zecchina, A. FTIR Spectroscopy and Thermodynamics of CO and H_2 Adsorbed on γ-, δ- and α-Al_2O_3. *Phys. Chem. Chem. Phys.* **2010**, *12*, 6474−82.
(51) Reller, A.; Cocke, D. L. High Resolution Transmission Electron Microscopic (HRTEM) Determination of the Preferentially Exposed Faces on γ-Al_2O_3 and η-Al_2O_3. *Catal. Lett.* **1989**, *2*, 91−95.
(52) Marchese, L.; Bordiga, S.; Coluccia, S.; Martra, G.; Zecchina, A. Structure of the Surface Sites of δ-Al_2O_3 as Determined by High-Resolution Transmission Electron Microscopy, Computer Modelling and Infrared Spectroscopy of Adsorbed CO. *J. Chem. Soc., Faraday Trans.* **1993**, *89*, 3483−3489.
(53) Wischert, R.; Coperet, C.; Delbecq, F.; Sautet, P. Optimal Water Coverage on Alumina: A Key to Generate Lewis Acid-Base Pairs that are Reactive Towards the C-H Bond Activation of Methane. *Angew. Chem., Int. Ed.* **2011**, *50*, 3202−3205.
(54) Larmier, K.; Chizallet, C.; Cadran, N.; Maury, S.; Abboud, J.; Lamic-Humblot, A. F.; Marceau, E.; Lauron-Pernot, H. Mechanistic Investigation of Isopropanol Conversion on Alumina Catalysts: Location of Active Sites for Alkene/Ether Production. *ACS Catal.* **2015**, *5*, 4423−4437.
(55) Larmier, K.; Nicolle, A.; Chizallet, C.; Cadran, N.; Maury, S.; Lamic-Humblot, A.-F.; Marceau, E.; Lauron-Pernot, H. Influence of Coadsorbed Water and Alcohol Molecules on Isopropyl Alcohol Dehydration on γ-Alumina: Multiscale Modeling of Experimental Kinetic Profiles. *ACS Catal.* **2016**, *6*, 1905−1920.
(56) Hu, J. Z.; Kwak, J. H.; Wang, Y.; Hu, M. Y.; Turcu, R. V.; Peden, C. H. F. Characterizing Surface Acidic Sites in Mesoporous-Silica-Supported Tungsten Oxide Catalysts Using Solid-State NMR and Quantum Chemistry Calculations. *J. Phys. Chem. C* **2011**, *115*, 23354−23362.
(57) Karakonstantis, L.; Matralis, H.; Kordulis, C.; Lycourghiotis, A. Tungsten−Oxo-Species Deposited on Alumina. II. Characterization and Catalytic Activity of Unpromoted W(vi)/γ-Al_2O_3 Catalysts Prepared by Equilibrium Deposition Filtration (EDF) at Various pH's and Non-Dry Impregnation (NDI). *J. Catal.* **1996**, *162*, 306−319.

DOI: 10.1021/acs.jpcc.6b09060
J. Phys. Chem. C 2016, 120, 23093−23103

(58) Thomas, R. Characterization of γ-Alumina-Supported Molybdenum Oxide and Tungsten Oxide; Reducibility of the Oxidic State Versus Hydrodesulfurization Activity of the Sulfided State. *J. Catal.* **1982**, *76*, 241−253.
(59) Martín, C.; Malet, P.; Solana, G.; Rives, V. Structural Analysis of Silica-Supported Tungstates. *J. Phys. Chem. B* **1998**, *102*, 2759−2768.
(60) Benitez, V. M.; Querini, C. A.; Fígoli, N. S.; Comelli, R. A. Skeletal Isomerization of 1-Butene on WOx/γ-Al_2O_3. *Appl. Catal., A* **1999**, *178*, 205−218.
(61) Carniti, P.; Gervasini, A.; Aurox, A. Energy Distribution of Surface Acid Sites of Metal Oxides. *J. Catal.* **1994**, *150*, 274−283.
(62) Busca, G. The Surface Acidity of Solid Oxides and Its Characterization by IR Spectroscopic Methods. An Attempt at Systematization. *Phys. Chem. Chem. Phys.* **1999**, *1*, 723−736.
(63) Kim, Y. K.; Dohnálek, Z.; Kay, B. D.; Rousseau, R. Competitive Oxidation and Reduction of Aliphatic Alcohols over $(WO_3)_3$ Clusters. *J. Phys. Chem. C* **2009**, *113*, 9721−9730.
(64) Kim, J.; Bondarchuk, O.; Kay, B. D.; White, J. M.; Dohnálek, Z. Preparation and Characterization of Monodispersed WO_3 Nanoclusters on TiO_2(110). *Catal. Today* **2007**, *120*, 186−195.

DOI: 10.1021/acs.jpcc.6b09060
J. Phys. Chem. C 2016, 120, 23093−23103